Check for updates

ADVANCED OPTICAL MATERIALS
www.advopticalmat.de

Independent Multiple-Optical-Parameter Modulations Enabled by Manipulating the Separate Levels of a Hierarchical Structure

*Cheng Ouyang, Quan-Ming Chen, Zhi-Yao Xie, Chun-Ting Xu, Qi-Guang Wang, Zhi-Gang Zheng, Dan Luo, Yan-Qing Lu, and Wei Hu**

Owing to their intrinsic multiple physical dimensions and high parallelism, photons are superior to electrons when they act as information carriers. The independent and dynamic spatial modulations of multiple optical parameters of light are highly pursued in vital fields such as supercomputing, constellation satellite and optical communications, virtual/augmented reality, and holographic displays. To date, it is still challenging to accomplish this urgent task with a single element. Here, multiple optical parameter modulations are carried out via manipulation of the separate levels of a hierarchical structure. Photopatterning, light irradiation, and an electric field are adopted to regulate the patterned crystallizations, lattice constants, and tilt angles of blue-phase liquid crystals (BPLCs). As the optical parameters are associated with the individual structural features, it enables binary reflectance and spatial geometric phase modulations, reversable wavelength shifting, and continuous reflectance variations with excellent independency. This work unlocks the multi-degree modulation of light and addresses the miniaturization, integration, and dynamic and multifunctional tendencies of rapidly growing optical informatics. Owing to its merits of omnidirectional, independent control, and dynamic response, it may dramatically upgrade the performance of existing optics.

1. Introduction

Photons are superior to electrons when they act as information carriers owing to their intrinsic multiple physical dimensions and high parallelism. The independent and dynamic modulations of multiple optical parameters of light are highly pursued in vital fields such as supercomputing, constellation satellite and optical communications, virtual/augmented reality, and holographic displays, where the multiplexing of multiple dimensions brings much higher capability. Optical functions are usually realized through spatially modulating the optical parameters, such as amplitude, phase, and wavelength, via light-matter interactions. The independent manipulation of individual optical parameters is highly demanded in advanced optical applications. Moreover, photonic technology is developing toward miniaturization, integration, multifunctionality, and adaptation. Researchers have paid a lot of attention to exploiting new materials and elements for multi-degree spatial light modulation meeting with this tendency. Metamaterials[1] and metasurfaces,[2] which regulate electromagnetic waves by tailoring the geometry of subwavelength metal or dielectric metaatoms, are considered the most attractive breakthroughs. Metadevices can modulate the multiple parameters of light with high flexibility within a wavelength comparable thickness; however, they are lack of tunability once fabricated. To achieve dynamic functions, heterogeneous integration, which is costly and complicated, of active materials such as phase change materials,[3] micro-electro-mechanical systems,[4] 2D materials,[5] semiconductors,[6] and liquid crystals (LCs)[7] has been adopted. Actually, LC itself is an ideal candidate for dynamic planar optics thanks to its responsiveness to the multiple external fields.

The dominant TFT-LCD with up to 4k or 8k resolution verifies the high parallelism in the light processing of LC techniques.[8] The high resolution can be further minimized to a chip with a size smaller than a half inch in near-eye displays including AR, VR and MR.[9] LCs exhibit excellent optical anisotropy over a super broadband. Therefore, in addition to information displays, it has also been utilized for wavelength selective switches in all-optical interconnections,[10] acquisition, pointing, and tracking systems[11] in satellite-based communications, as well as dynamic terahertz imaging and beam steering. LC on silicon is a

C. Ouyang, Q.-M. Chen, Z.-Y. Xie, C.-T. Xu, Q.-G. Wang, Y.-Q. Lu, W. Hu
National Laboratory of Solid State Microstructures
Jiangsu Physical Science Research Center
College of Engineering and Applied Sciences
Nanjing University
Nanjing 210023, China
E-mail: huwei@nju.edu.cn
Q.-M. Chen, D. Luo
Department of Electrical & Electronic Engineering
Southern University of Science and Technology
Shenzhen 518055, China
Z.-G. Zheng
College of Physics
East China University of Science and Technology
Shanghai 200237, China
The ORCID identification number(s) for the author(s) of this article can be found under https://doi.org/10.1002/adom.202402844

DOI: 10.1002/adom.202402844

 © 2024 Wiley-VCH GmbH

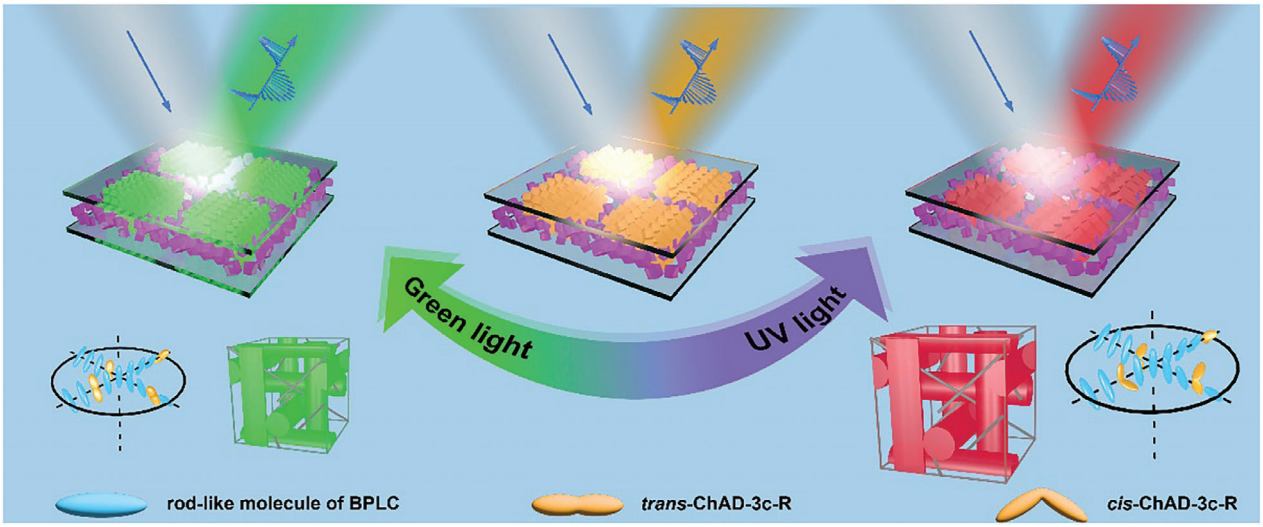

Figure 1. Schematic illustration of the mechanism for UV/Green light-driven wavelength shifting of a chiral molecular switch doped and photopatterned BPLC.

widely used spatial light modulator that can modulate polarization, amplitude and phase separately via electrically addressing millions of pixels.[12] Although the impressive progress in spatial light modulators as well as meta devices, it is still challenging to accomplish independent and dynamic modulations of multiple optical parameters with a single element. Recently, researchers have attempted to manipulate the different levels of LC hierarchical structures in order to modulate the distinct parameters of light.[13] A cholesteric LC (CLC) spontaneously assembles into a 1D chiral photonic crystal, whose chirality, pitch and initial azimuth determine the spin, wavelength and geometric phase of the selectively reflected light.[14] One can freely program the geometric phase by presetting the initial alignment of the CLC via photoalignment,[15] while the working wavelength can be continuously customized by thermally, optically or electrically tuning the helical pitch. It enables the independent control of the phase and wavelength.[14c,16] Additionally, the spin conversion is also demonstrated via optically reversing the helicity.[17] Compared with 1D CLC, blue phase LCs (BPLCs) self-assemble into a 3D photonics crystals, further extending the structural hierarchy.[18] This entropy dominated system is usually unstable, giving rise to randomly oriented lattices.[19] Researchers have introduced external physical fields such as unidirectional surface anchoring,[20] long lasting electric field,[21] surface acoustic waves,[22] and gradient temperature scanning[23] to suppress the random nucleation to obtain a large-area monodomain. By further introducing patterned alignments, the shapes of BP crystallographic domains can be arbitrarily tailored.[20b] Very recently, the mapping relationship between the chirality/lattice constant/lattice orientation of a BPLC and the spin/wavelength/geometric phase of light has been disclosed. The unique property makes BPLC naturally suitable for omnidirectional multi-degree light modulation.[24] If one can accurately and dynamically manipulate separate levels of the BPLC hierarchical structure, the multiple optical parameters are expected to be modulated independently. It may pave a bright way for revolutionary optics which will drastically accelerate the optical informatics.

We investigate the evolution of separate levels of BPLC hierarchical structures under different physical stimulations, and realize the reversable and independent manipulation of the multiple parameters of light, accordingly. The reversible photoisomerization of a chiral dopant is carried out by alternating ultraviolet (UV) and green light irradiation. This phenomenon causes the wind and unwind of the helical structure, and the lattice constant changes correspondingly and thus leading to a reversable wavelength shifting. An alternating current (AC) electric field is applied vertically to tune the tilt angle of the whole LC, causing a continuous variation of reflectance in the selective photonics band. The photoalignment is adopted to pattern the BP crystallizations, which enables the spatial modulation of both the reflectance and the geometric phase. Moreover, the patterns can be rewritten by linearly polarized UV when a saturated electric field is applied. The separate control of the multi optical parameters unlocks the freedom in multiple physical dimensions, and has great significance in the rapidly increasing optical informatics.

2. Results and Discussion

The evolution of discrete levels of BPLC hierarchical structures to different stimuli and corresponding optical parameter modulations are systematically investigated. Since alignment facilitates the growth of BPLC monodomains, photopatterning enables a free control on the shape of crystallographic domains.[20b] The monodomain in the aligned regions exhibits a much higher reflectance within the photonics bandgap (PBG) than the polydomain in the unaligned regions (Figure S1, Supporting Information), and thus colored patterns consistent with the preset alignments are generated. **Figure 1** schematically illustrates a photopatterned tetragonal lattice of square domains. A chiral molecular switch is doped into the BPLC, which isomerizes reversibly between the trans-form and the cis-form under UV and green light irradiation. The molecular deformation changes the helical twisting power of the BPLC, induces the unwinding and winding of the helical structure, and finally varies the lattice constants of

© 2024 Wiley-VCH GmbH

21951071, 2025, 11, Downloaded from https://advanced.onlinelibrary.wiley.com/doi/10.1002/adom.202402844 by Nanjing University, Wiley Online Library on [13/01/2026]. See the Terms and Conditions (https://onlinelibrary.wiley.com/terms-and-conditions) on Wiley Online Library for rules of use; OA articles are governed by the applicable Creative Commons License

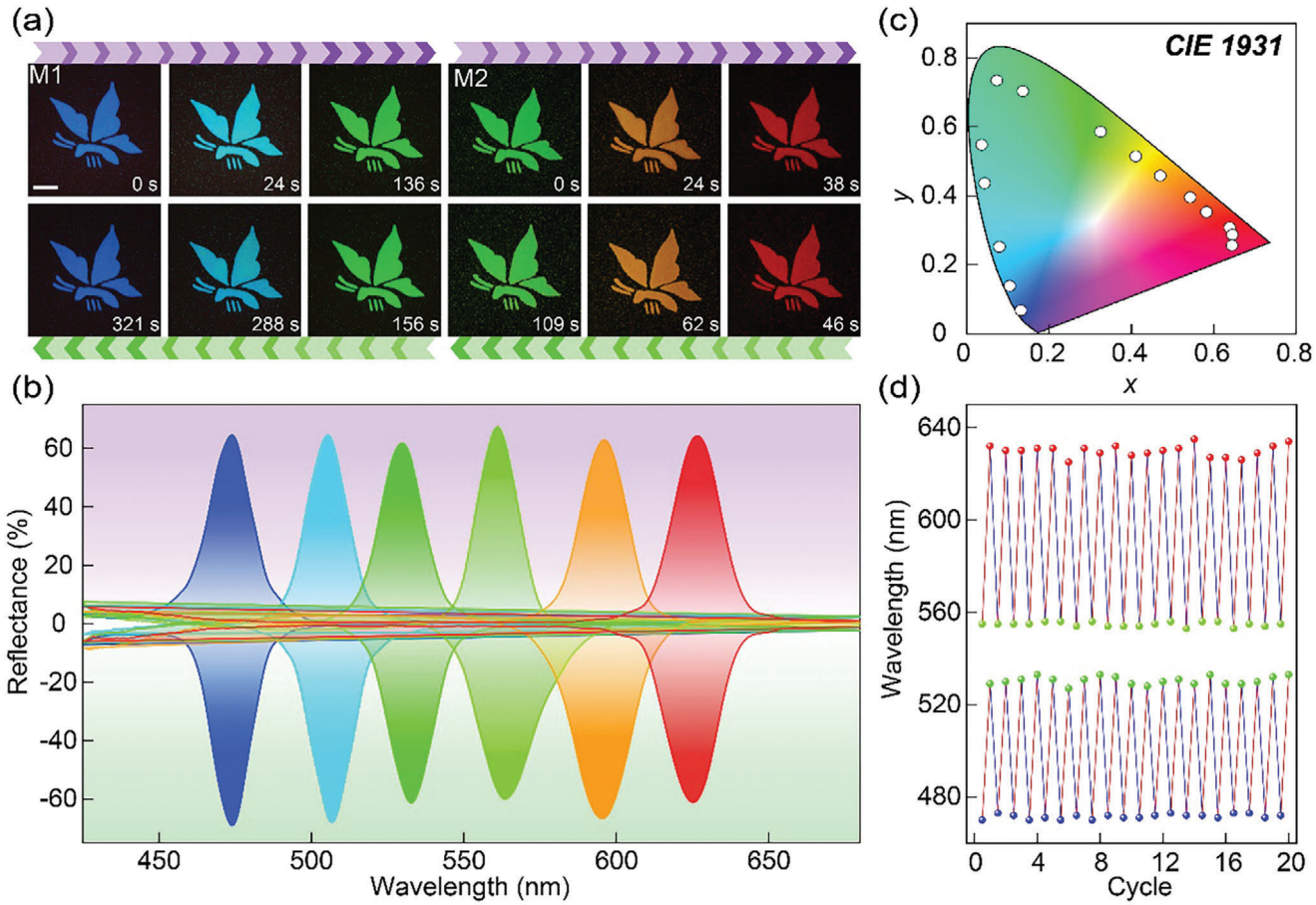

Figure 2. Independent modulations of spatial reflection and wavelength. a) POM images of reversible photochromic butterflies of samples M1 and M2, respectively. The lower right corner reveals the corresponding irradiation time. b) Reflection spectra from the butterflies in (a). c) Chromatic coordinates of the samples calculated from the reflection spectra during the UV/green light irradiation process in the CIE 1931 diagram. d) Anti-fatigue strength after 20 UV/green light irradiation cycles. The scale bar indicates 200 μm for all micrographs.

the BPLC. The PBG changes accordingly and results in a continuous shift in the reflected wavelengths. By controlling the UV and green light doses, the colors of BPLC patterns can be customized.

A butterfly is recorded into the photoalignment agent SD1 by a digital micromirror device based dynamic photoexposure system,[25] and then a BPLC doped with a molecular switch ChAD-3c-R is filled into the cell in the isotropic state. Owing to the limited helical twisting power change of the adopted molecular switch, two BP samples of different compositions (M1 and M2, their phase transition behaviors are shown in Figure S2, Supporting Information) are prepared to demonstrate the reversible color variation from blue to green and from green to red, respectively. As exhibited in **Figure** 2a, after gently cooling to the BPI state at-0.3 °C min^{-1} with Kossel diffraction shown in Figure S1 (Supporting Information), highly reflective butterfly-shaped monodomains are observed via polarized optical microscopy (POM). The initial central wavelength of Bragg reflection for M1 is 475 nm. Upon UV irradiation at 0.48 mW cm^{-2} for 136 s, the wavelength continuously redshifted to 530 nm. Then the sample is irradiated by green light at 0.48 mW cm^{-2} for 165 s, and the wavelength shifts back to the initial 475 nm. For M2, the shift range of the central wavelength moves to 555 and 630 nm, and the UV/green light irradiation time changes to 38/63 seconds due to the lower viscosity of M2 (Figure S3, Supporting Information). The response can be significantly improved by increasing the irradiation light intensity. During the irradiation process, a uniform and continuous color variation is observed, while the shape of the butterfly remains unchanged. The reflection spectra are well recovered during the reversible UV/green light irradiation, suggesting the arrangement of BPLC cubic lattices is accurately controlled during the irradiations (Figure 2b). M1 and M2 work together to cover the visible band. We calculate the chromatic coordinates according to the reflection spectra, and all the points are located near the edge of the CIE 1931 diagram (Figure 2c). This shows the excellent monochromaticity of these BPLC patterns.

We expose stripes with gradient widths to test the spatial resolution of such patterns. The precision of the optical patterning system is 1 μm. Stripes in width of 4 μm are successfully fabricated in 8-μm BP I, thanks to its much weaker epitaxial growth compared to BP II. We monitor the width fluctuations of a 48 μm stripe along the *x*- and *y*-axes, respectively. During the irradiation process, variations of stripe widths are negligible. Notably, as M2 is a weak chiral system, more significant epitaxial growth

© 2024 Wiley-VCH GmbH

21951071, 2025, 11, Downloaded from https://advanced.onlinelibrary.wiley.com/doi/10.1002/adom.202402844 by Nanjing University, Wiley Online Library on [13/01/2026]. See the Terms and Conditions (https://onlinelibrary.wiley.com/terms-and-conditions) on Wiley Online Library for rules of use; OA articles are governed by the applicable Creative Commons License

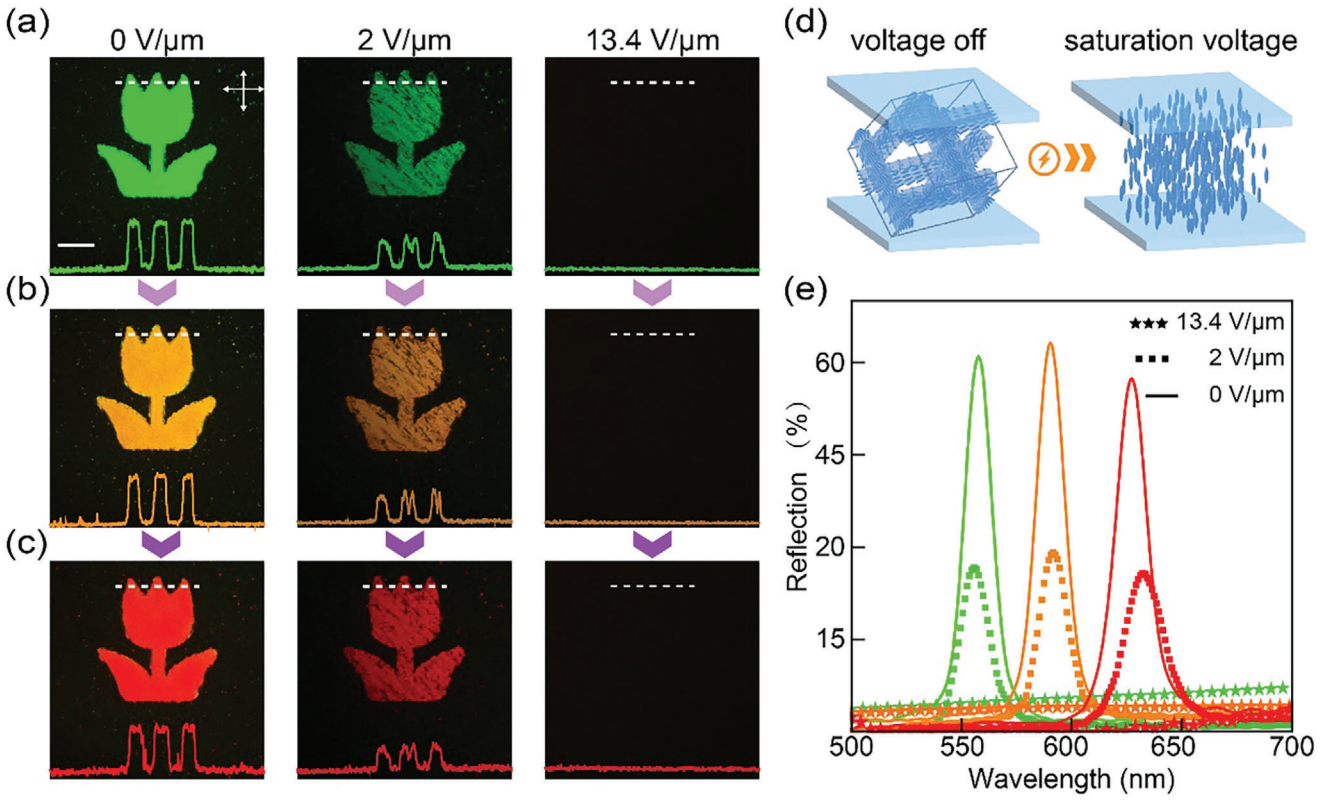

Figure 3. Electric-driven continuous reflectance modulation. Electric-tuned grayscales of different colored tulips at voltages of 0 V/μm, 2 V/μm, and 13.4 V/μm, respectively. a) green, b) orange, c) red. The corresponding intensity profiles in the white dashed lines marked regions are presented at the bottom of each image. d) Schematic diagram of the deformation of the LC director field under different electric fields. e) Reflection spectra from the tulips with different voltages applied. The scale bar indicates 100 μm for all micrographs.

is exhibited as compared to M1. The single-micron scale epitaxial growth during the irradiation indicates a pronounced independency between the wavelength shift and the binary reflective pattern (Figure S4, Supporting Information). The maximum reflectance for circularly polarized light of the same handedness to the helical structure is 65%, which can be further improved by enlarging the cell gap. However, a thinner cell gap benefits from high spatial resolution. Excellent wavelength reversibility is demonstrated even after 20 cycles of UV/green light irradiation (Figure 2d). Moreover, the reflection spectra of M1 and M2 are almost the same as the initial states (Figure S5, Supporting Information), indicating a reliable color gamut performance due to the excellent fatigue strength of the BPLCs.

The electric-driven reflectance variation of a photopatterned tulip is demonstrated to verify the independent modulation of the reflectance, wavelength shifting, and spatial patterning. As shown in **Figure** 3a–c, guided by the local photoalignment, a green tulip is grown in the voltage-off state (0 V/μm), and the reflective color redshifts (green, yellow to red) under UV irradiation as mentioned previously. When an AC electric field of 2 V/μm is applied vertically, the tulip changes in the same color sequence along with the UV irradiation. However, decreased reflectance is exhibited due to the total tilt angle increase in the LC director field is caused by the electric field, which reduces the birefringence of the BPLC. Moreover, the central wavelengths of the reflection spectra are almost unchanged under a weak electric field, indicating that the lattice constant is maintained (Figure 3e). When the field reaches 13.4 V/μm, the helical structure is completely unwound, in which case the LC enters a homeotropic state (Figure 3d), leading to a dark state under a POM. The profiles reveal the intensity distributions marked with white dashed lines, suggesting that grayscale can be achieved by applying different voltages. During the UV-irradiating and electric-driving process, the shape of the tulip remains very well, verifying the excellent independency of the reflectance modulation on wavelength shifting and spatial patterning. Notably, under weak electric field conditions, the BPLC lattice is undestroyed, and the tulip will completely recover after the field is removed. The high electric field (for example, saturated voltage) causes the lattice to collapse, and the tulip cannot return to the initial state directly by removing the voltage unless it undergoes thermal recycling. The electric-driven reflectance modulation of a blue tulip based on M1 is also presented, and the central wavelengths of the reflection spectra also remain when the reflectance varies under an electric field (Figure S6, Supporting Information).

The spatial geometric phase modulation can be carried out by presetting the BP lattice azimuth via a step-by-step exposure. We utilize the Gerchberg-Saxton algorithm to design the hologram of a cartoon calf (**Figure** 4a). Here, the configuration of the BPLC is much more complicated than that of the photopatterned BP monodomain. The central wavelengths reflected by BP holograms can be reversibly shifted under UV/green light

© 2024 Wiley-VCH GmbH

21951071, 2025, 11, Downloaded from https://advanced.onlinelibrary.wiley.com/doi/10.1002/adom.202402844 by Nanjing University, Wiley Online Library on [13/01/2026]. See the Terms and Conditions (https://onlinelibrary.wiley.com/terms-and-conditions) on Wiley Online Library for rules of use; OA articles are governed by the applicable Creative Commons License

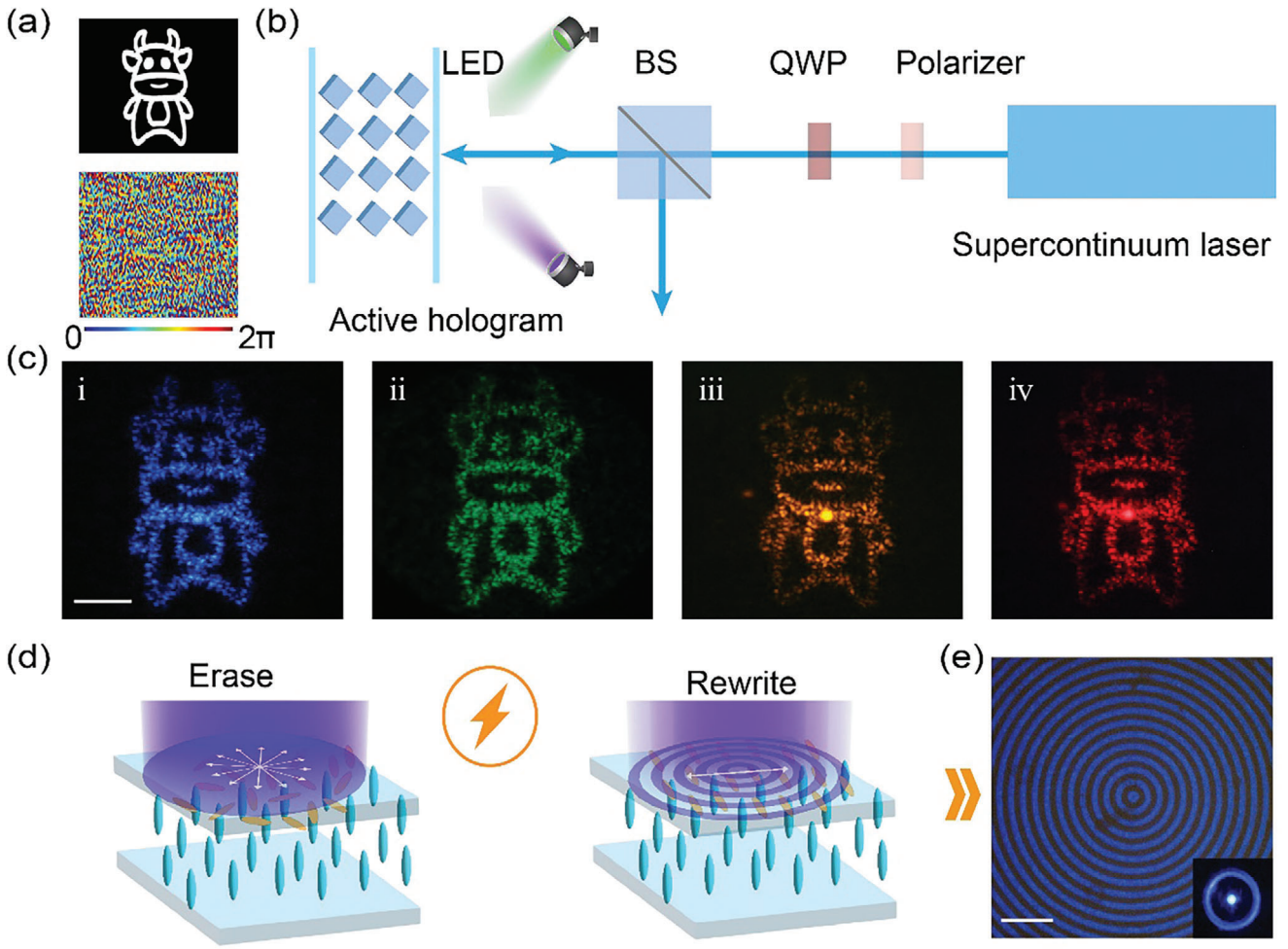

Figure 4. Geometric phase encoding and rewriting. a) Calf cartoon and corresponding hologram. b) Optical setup for characterizing the active holography. c) Central wavelength shifting of the generated calf: i) 470 nm, ii) 530 nm, iii) 600 nm and iv) 630 nm. The scale bar indicates 3 mm for all images. d) Scheme of the erasing and rewriting of the alignment when a saturated electric field is applied to the sample. e) A binary ring grating rewritten from the calf hologram; the insert shows the corresponding diffraction pattern. The scale bar indicates 200 μm.

irradiation, respectively (Figure S7a, Supporting Information). Narrowband reflection spectra are captured from the patterned samples (Figure S7b, Supporting Information), indicating the high quality of the formed complex lattices. A reflective optical setup, as shown in Figure 4b, is adopted to characterize the performance of the sample. During the irradiation process, light with a wavelength falling into the photonics band gap is selectively diffracted to generate different colored calf patterns (Figure 4c). The blue, green, orange, and red calves (M1 for the former two colors and M2 for the other colors) are presented as examples. A high diffraction efficiency of up to 83% was achieved (Figure S6c, Supporting Information), further verifying the high quality of the generated holograms. The encoded hologram can be erased by a blue LED with an electric field of 3.0 V μm^{-1} applied to drive the LC of M1 into the homeotropic state. Then, we rewrote binary circular gratings into the same sample via a new photopatterning process (Figure 4d). After the electric field and thermal recycling are removed, a binary ring pattern is formed, and its diffraction ring is recorded, as shown in Figure 4e. Here, an amplitude pattern is given as an example, and the geometric phase pattern can also be rewritten. It enables the rewritability of both the spatial amplitude and the geometric phase.

In this work, by manipulating the different levels of the hierarchical structure of an ordered BPLC with distinct physical fields, separate optical parameters of light are reversibly and independently modulated. Both the shape of the BP crystallographic monodomains and their local lattice orientations are preprogrammed by photopatterning and can be further rewritten. It enables the reconfigurable spatial modulations of both the binary reflectance and the geometric phase. UV/green light irradiation over the molecule switch doped BP leads to the reversible helical pitch tuning and reflective wavelength shifting, accordingly. The vertically applied electric field changes the tilt angle of the BPLC and thus modulates the reflectance within the photonic bandgap. The dynamic tuning and independent controlling of the wavelength, reflectance, and geometric phase are demonstrated, which unlocks the multi-degree light modulation within a single element. Here, a uniform electric field and light irradiation are adopted for easy demonstration; however, it can be rationally expected that pixelated electrically driven and optically

© 2024 Wiley-VCH GmbH

21951071, 2025, 11, Downloaded from https://advanced.onlinelibrary.wiley.com/doi/10.1002/adom.202402844 by Nanjing University, Wiley Online Library on [13/01/2026]. See the Terms and Conditions (https://onlinelibrary.wiley.com/terms-and-conditions) on Wiley Online Library for rules of use; OA articles are governed by the applicable Creative Commons License

addressed stimuli will significantly enhance the capability for multi-degree light modulation. It needs to be mentioned that the adopted photosensitive molecular switch keeps on thermally isomerizing even after the irradiation stops, making the reflective color cannot be fixed for a long time. Fortunately, this problem can be solved by introducing multi-stable molecular switches.[26] By introducing high-performance molecular switches and more sensitive photoalignment agents, the response can be drastically accelerated. Moreover, the wavelength tuning range can be extended to the whole visible range with a single material and the handedness conversion can also be accomplished, making the flip of light spins possible. In addition to the spin, the orbital angular momentum of light can also be modulated by encoding the proper geometric phase to the sample. Therefore, the BPLC may provide a promising and practical platform for multi-degree light modulation, with the merits of omnidirectional, separate control and dynamic response.

3. Conclusion

Dynamic multiple optical parameter modulations of light are demonstrated on the basis of manipulating the separate levels of BPLC hierarchical structures with electric-driven, UV/green irradiation, and photopatterning, separately. As the optical parameters are associated with individual structural features that can be controlled separately, here the spatial light modulation exhibited excellent parameter independency. It unlocks the freedom of multi-degree light modulation and is of great significance to the rapidly growing optical informatics.

4. Experimental Section

Materials: M1 was mixed with a host nematic LC TEB300 (Slichem, China), the chiral dopant R5011 (HTP = 110 μm^{-1} at 30 °C, NCLCP, China), ChAD-3C-R (BEAM, USA), the reactive mesogen RM257 (NCLCP, China), 2-ethylhexyl acrylate (EHA, Sigma–Aldrich, USA), and the only difference of M2 compared with M1 was the host nematic HTW114200-050 ($\Delta\epsilon$ = 10.9 at 1 kHz and 20 °C; Δn = 0.222 and n_e = 1.729 at 589 nm and 20 °C. HCCH, China). The weight ratios of the host nematic, R5011, Chad-3C-R, RM257, and EHA were both fixed at 88.5, 4, 1.5, 3, and 3 wt.%, respectively. The temperature was precisely controlled with an LTS 120 hot stage (Linkam, UK). The phase transition points for M1: isotropic (ISO)-48 °C-blue phase I (BP I)-37 °C-cholesteric (N^*); and M2: ISO-90 °C -BPI-82 °C-N^* (Figure S2, Supporting Information). UV/green light irradiations were carried out with 365 and 530 nm LEDs (Thorlabs, USA), separately.

Cell Fabrication: The indium–tin-oxide glass substrates were activated by UV-Ozone, then spin-coated with 0.3 wt.% photoalignment agent SD1 (NCLCP, China) solved in dimethylformamide (DMF, Sigma–Aldrich, USA). After baking at 100 °C for 10 min, two substrates were separated by 8-μm spacers and sealed with epoxy glue. The photoalignment was performed with a 1920 × 1080 pixelated digital micromirror device-based microlithography system (NCLCP, China).

Characterizations: The reflection spectra were recorded with a spectrometer (PG2000-pro, Ideaoptics, China). All the micrographs were captured under the reflective mode of a POM (Nikon 50i, Japan), and the Kossel diffraction was observed with a microscope (Olympus, BX51, Japan). Monochromatic beams were output by a supercontinuum laser (SuperK EVO, NKT Photonics, Denmark) and selected by a multichannel acousto-optic tunable filter (SuperK SELECT, NKT Photonics, Denmark). A digital camera (EOS M, Canon, Japan) was used to capture the diffraction patterns. The function generator (33522B, Agilent, USA) and voltage amplifier (2340, TEGAM, USA) provide an electric field.

Supporting Information

Supporting Information is available from the Wiley Online Library or from the author.

Acknowledgements

C.O. and Q.C. contributed equally to this work. The authors gratefully acknowledge the support of the National Key Research and Development Program of China (2022YFA1203700), the National Natural Science Foundation of China (NSFC) (T2488302, 62035008 and 62405127), the Natural Science Foundation of Jiangsu Province (BK20233001), Fundamental Research Funds for the Central Universities (021314380244), and the Postdoctoral Fellowship Program of CPSF under Grant Number (GZC20240640). The authors gratefully appreciate JCOPTIX for providing the optical test equipment. The authors appreciate Dei-Wei Zhang and Jin-Bing Wu for their constructive discussions.

Conflict of Interest

The authors declare no conflict of interest.

Data Availability Statement

The data that support the findings of this study are available from the corresponding author upon reasonable request.

Keywords

blue-phase liquid crystals, liquid crystal optics, self-organizations, spatial light modulations

Received: October 21, 2024
Revised: December 4, 2024
Published online: December 30, 2024

[1] a) K. Bertoldi, V. Vitelli, J. Christensen, M. van Hecke, *Nat. Rev. Mater.* **2017**, *2*, 17066; b) D. Schurig, J. J. Mock, B. J. Justice, S. A. Cummer, J. B. Pendry, A. F. Starr, D. R. Smith, *Science* **2006**, *314*, 977.
[2] a) A. Tittl, A. Leitis, M. Liu, F. Yesilkoy, D. Y. Choi, D. N. Neshev, Y. S. Kivshar, H. Altug, *Science* **2018**, *360*, 1105; b) N. Yu, F. Capasso, *Nat. Mater.* **2014**, *13*, 139.
[3] X. Sha, K. Du, Y. Zeng, F. Lai, J. Yin, H. Zhang, B. Song, J. Han, S. Xiao, Y. Kivshar, Q. Song, *Sci. Adv.* **2024**, *10*, eadn9017.
[4] M. Manjappa, P. Pitchappa, N. Singh, N. Wang, N. I. Zheludev, C. Lee, R. Singh, *Nat. Commun.* **2018**, *9*, 4056.
[5] a) Q. S. Li, X. D. Cai, T. Liu, M. Jia, Q. Wu, H. Y. Zhou, H. H. Liu, Q. Q. Wang, X. H. Ling, C. Chen, F. Ding, Q. He, Y. B. Zhang, S. Y. Xiao, L. Zhou, *Nanophotonics* **2022**, *11*, 2085; b) T. T. Kim, S. S. Oh, H. D. Kim, H. S. Park, O. Hess, B. Min, S. Zhang, *Sci. Adv.* **2017**, *3*, e1701377.
[6] J. Gu, R. Singh, X. Liu, X. Zhang, Y. Ma, S. Zhang, S. A. Maier, Z. Tian, A. K. Azad, H. T. Chen, A. J. Taylor, J. Han, W. Zhang, *Nat. Commun.* **2012**, *3*, 1151.
[7] a) S. Q. Li, X. Xu, R. Maruthiyodan Veetil, V. Valuckas, R. Paniagua-Dominguez, A. I. Kuznetsov, *Science* **2019**, *364*, 1087; b) Z. X. Shen, S. H. Zhou, X. A. Li, S. J. Ge, P. Chen, W. Hu, Y. Q. Lu, *Adv. Photonics* **2020**, *2*, 036002; c) S. Q. Zhu, Q. Jiang, Y. T. Wang, L. L. Huang, *Nanophotonics* **2023**, *12*, 1169; d) Q. G. Wang, S. J. Ge, H. G. Yu, W. Hu, *Laser Photonics Rev.* **2024**, *18*, 2400869.

© 2024 Wiley-VCH GmbH

21951071, 2025, 11, Downloaded from https://advanced.onlinelibrary.wiley.com/doi/10.1002/adom.202402844 by Nanjing University, Wiley Online Library on [13/01/2026]. See the Terms and Conditions (https://onlinelibrary.wiley.com/terms-and-conditions) on Wiley Online Library for rules of use; OA articles are governed by the applicable Creative Commons License

[8] D. Yang, S. Wu, *Fundamentals of liquid crystal devices*, John Wiley & Sons, Hoboken, New Jersey **2014**.
[9] K. Yin, E. L. Hsiang, J. Zou, Y. Li, Z. Yang, Q. Yang, P. C. Lai, C. L. Lin, S. T. Wu, *Light Sci. Appl.* **2022**, *11*, 161.
[10] a) Y. Ma, L. Stewart, J. Armstrong, I. G. Clarke, G. Baxter, *J. Lightwave Technol.* **2020**, *39*, 896; b) M. Wang, L. J. Zong, L. Mao, A. Marquez, Y. B. Ye, H. Zhao, F. J. V. Caballero, *Photonics* **2017**, *4*, 22.
[11] Y. B. Shi, J. M. Zhang, Z. Zhang, *Photonic Sens.* **2016**, *6*, 289.
[12] Z. C. Zhang, Z. You, D. P. Chu, *Light Sci. Appl.* **2014**, *3*, e213.
[13] a) P. Chen, B. Y. Wei, W. Hu, Y. Q. Lu, *Adv. Mater.* **2020**, *32*, 1903665; b) J. B. Wu, S. B. Wu, H. M. Cao, Q. M. Chen, Y. Q. Lu, W. Hu, *Adv. Opt. Mater.* **2022**, *10*, 2201015.
[14] a) M. Rafayelyan, G. Tkachenko, E. Brasselet, *Phys. Rev. Lett.* **2016**, *116*, 253902; b) R. Barboza, U. Bortolozzo, M. G. Clerc, S. Residori, *Phys. Rev. Lett.* **2016**, *117*, 053903; c) C. T. Xu, B. H. Liu, C. Peng, Q. M. Chen, P. Chen, P. Z. Sun, Z. G. Zheng, Y. Q. Lu, W. Hu, *Adv. Opt. Mater.* **2022**, *10*, 2201088.
[15] J. Kobashi, H. Yoshida, M. Ozaki, *Nat. Photonics* **2016**, *10*, 389.
[16] S. L. Li, Z. Y. Chen, P. Chen, W. Hu, C. Huang, S. S. Li, X. Hu, Y. Q. Lu, L. J. Chen, *Light Sci. Appl.* **2024**, *13*, 27.
[17] P. Chen, L. L. Ma, W. Hu, Z. X. Shen, H. K. Bisoyi, S. B. Wu, S. J. Ge, Q. Li, Y. Q. Lu, *Nat. Commun.* **2019**, *10*, 2518.
[18] a) K. Bagchi, T. Emersic, J. A. Martinez-Gonzalez, J. J. de Pablo, P. F. Nealey, *Sci. Adv.* **2023**, *9*, eadh9393; b) J. Liu, W. Liu, B. Guan, B. Wang, L. Shi, F. Jin, Z. Zheng, J. Wang, T. Ikeda, L. Jiang, *Nat. Commun.* **2021**, *12*, 3477; c) Y. Yang, L. Wang, H. Yang, Q. J. S. S. Li, *Small Sci.* **2021**, *1*, 2100007.
[19] J. Yang, W. Zhao, W. He, Z. Yang, D. Wang, H. Cao, *J. Mater. Chem. C* **2019**, *7*, 13352.
[20] a) P. Nayek, H. Jeong, H. R. Park, S. W. Kang, S. H. Lee, H. S. Park, H. J. Lee, H. S. Kim, *Appl. Phys. Express* **2012**, *5*, 051701; b) Z. G. Zheng, C. L. Yuan, W. Hu, H. K. Bisoyi, M. J. Tang, Z. Liu, P. Z. Sun, W. Q. Yang, X. Q. Wang, D. Shen, Y. Li, F. Ye, Y. Q. Lu, G. Li, Q. Li, *Adv. Mater.* **2017**, *29*, 8; c) M. Wang, C. Zou, J. Sun, L. Zhang, L. Wang, J. Xiao, F. Li, P. Song, H. Yang, *Adv. Funct. Mater.* **2017**, *27*, 1702261.
[21] T. H. Lin, D. Y. Guo, C. W. Chen, T. M. Feng, W. X. Zeng, P. C. Chen, L. Y. Wu, W. M. Guo, L. M. Chang, H. C. Jau, C. T. Wang, T. J. Bunning, I. C. Khoo, *Nat. Commun.* **2024**, *15*, 7038.
[22] R. Suryantari, Y. H. Shih, H. Y. Chen, C. S. Wu, C. Y. Huang, *Opt. Lett.* **2023**, *48*, 77.
[23] C. W. Chen, C. T. Hou, C. C. Li, H. C. Jau, C. T. Wang, C. L. Hong, D. Y. Guo, C. Y. Wang, S. P. Chiang, T. J. Bunning, I. C. Khoo, T. H. Lin, *Nat. Commun.* **2017**, *8*, 727.
[24] Q. M. Chen, X. Y. Wang, C. T. Xu, H. C. Chu, H. G. Yu, C. Ouyang, Y. Lai, Z. G. Zheng, X. Liang, Y. Q. Lu, W. Hu, *Laser Photonics Rev.* **2024**, *18*, 2301283.
[25] P. Chen, L. L. Ma, W. Duan, J. Chen, S. J. Ge, Z. H. Zhu, M. J. Tang, R. Xu, W. Gao, T. Li, *Adv. Mater.* **2018**, *30*, 1705865.
[26] a) Z. G. Zheng, H. L. Hu, Z. P. Zhang, B. H. Liu, M. Q. Li, D. H. Qu, H. Tian, W. H. Zhu, B. Feringa, *Nat. Photonics* **2022**, *16*, 226; b) H. L. Hu, M. He, X. S. Liang, M. Q. Li, C. L. Yuan, B. H. Liu, X. Liu, Z. G. Zheng, W. H. Zhu, *Matter* **2023**, *6*, 3927.

 © 2024 Wiley-VCH GmbH

21951071, 2025, 11, Downloaded from https://advanced.onlinelibrary.wiley.com/doi/10.1002/adom.202402844 by Nanjing University, Wiley Online Library on [13/01/2026]. See the Terms and Conditions (https://onlinelibrary.wiley.com/terms-and-conditions) on Wiley Online Library for rules of use; OA articles are governed by the applicable Creative Commons License